Gamma Ray Spectroscopy

Ian Rittersdorf
Nuclear Engineering & Radiological Sciences
ianrit@umich.edu

March 20, 2007

Contents

1 Abstract

In lab, a total of eight spectra were measured. From know values of gamma-ray energies, a calibration curve was plotted. The best fit line on the calibration curve proved that the MCA channels all had the same width of energy. The best fit line matched the data with a least squares fit of $R^2 = 1$. Using the HPGe detector in tandem with the MCA, all of the spectra were measured. All of their features, including photopeaks, summation peaks, annihilation peaks, and X-rays were indentified.

Analyzing the background count showed a large amount of ambient radiation. Many daughters from the 4n and the 4n + 2 decay chains were present in the count. Other notable background sources were ^{137}Cs and ^{40}K. These sources are also expected to be present; ^{40}K because of its large half-life and ^{137}Cs because of its man-made abundance.

Energy resolutions of this detector were plotted and shown to increase with increasing gamma-ray energy.

2 Introduction & Objectives

While a Geiger counter merely determines count rates for radiation, gamma spectroscopy has the ability to determine both the count rate and the energy of the radiation. This turns out to be extremely important as different radioiosotopes emit many gammas of differing energies. A gamma spectrum is created by taking measurements of emitted gamma-rays and processing them. A detector could identify an unknown radioisotope by identifying features on the gamma spectrum and comparing them to known spectra. The implications

of this are quite vast. In the field of homeland security, for example, a detector could gather information from a man's briefcase. If that man had an explosive device in his briefcase, features characteristic to explosive materials would show up on the gamma spectrum and the bomb would not make it past security. In this lab, the spectra of seven different sources will be measured. These spectra will be analyzed and the features that distinguish them from other spectra will identified.

3 Theory

Detecting X-rays and gamma-rays is not a direct process. X-ray and gamma-ray photons do not have an intrinsic charge and therefore do not create ionization or excitation of the medium it is passing through directly. Thus, the measurement of these photons is dependent on their interaction with the electrons of the medium. The incident photons will create fast electrons which we look at to understand the nature the of photon itself. These electrons will have a maximum energy that is equal to the energy of the incident gamma-ray on that electron. There are three manners in which the photon will interact with the medium that it is in that is of concern for gamma-ray spectroscopy: photoelectric absorption, Compton scattering, and pair production.

Because of the fact that the photons themselves are invisible to the detector, a detector needs to have a couple of specific functions. The first is to act as a medium that will have a high probability that an incident gamma-ray will interact within that medium. The second function of the detector is to accurately detect the fast electrons that are created.

The gas-filled detectors that have been used in the laboratory thus far are ineffective at detecting gamma-rays due to the lower stopping power of gases. Because of this, the switch

to semiconductor detectors has been made for this lab, but this will be discussed in a later section.

3.1 Gamma-Ray Interactions

A gamma-ray will interact with its medium in one of three different ways: photoelectric absorption, Compton scattering, and pair production. These different interactions change their probability of occurring depending on the energy of the gamma-ray and the atomic number of the material.

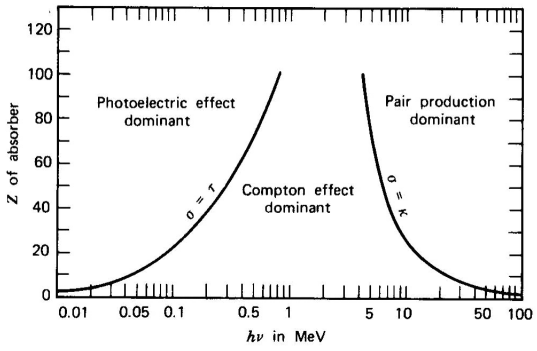

Figure 3.1: A graph depicting the various regions where the different gamma-ray interactions are dominant.

As can be seen from Figure 3.1, the photoelectric effect is dominant for low energy photons and high Z materials. Pair production is dominant for high energy photons and high Z materials. The Compton scattering interaction is dominant for moderate energies.

3.1.1 Photoelectric Absorption

In the photoelectric absorption, the incident photon disappears and a photoelectron is produced from one of the electron shells of the absorber. The kinetic energy that this electron carries off is $E_{e^-} = h\nu - E_b$, where E_b is the binding energy of the liberated electron in its original shell. This empty spot in the electron shell is quickly filled by electron rearrange-

ment. This process causes the binding energy, E_b, to be liberated as well. This energy is liberated in the form of a characteristic X-ray or an Auger electron.

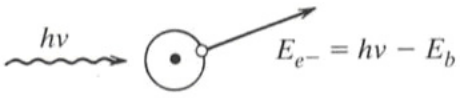

Figure 3.2: A depiction of photoelectric absorption

The photoelectric absorption interaction is the ideal interaction for gamma-ray spectroscopy. The photoelectron carries away most of the gamma-ray energy and then an X-ray or Auger electron carries away the remaining kinetic energy. Assuming an ideal detector, the sum of these energies will equal the energy of the original gamma-ray.

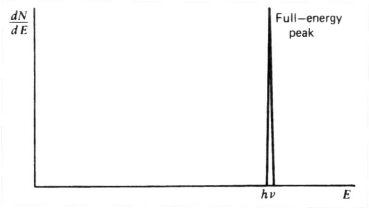

Figure 3.3: A single peak at a total electron energy corresponding to the energy of incident gamma-rays of a single energy.

This is desired for gamma-ray spectroscopy because we are interested in knowing the energies of the various gamma-rays that are emitted by a source. In Figure 3.3, we see what the ideal photopeak created by mono-energetic gamma-rays of a single energy looks like.

3.1.2 Compton Scattering

The Compton scattering interaction is the scattering of a gamma-ray off of a free or unbound electron, thus creating a scattered gamma-ray photon and a recoil electron. The energy of the incoming photon is divided between the scattered photon and the recoil nucleus by a relationship that is dependent on the scattering angle. The energy of the recoil electron is

$$E_{e^-} = h\nu - h\nu' \quad = \quad h\nu \left(\frac{(h\nu/m_0c^2)/(1 - cos(\theta))}{1 + (h\nu/m_0c^2)(1 - cos(\theta))} \right) \tag{1}$$

There are two extreme cases dictated by this equation: When $\theta \cong 0$, the scattered photon retains all of its energy and the recoil electron gains no energy. When $\theta = \pi$, the incident gamma-ray is backscattered and the recoil electron moves along the direction of incidence. This case is the case with the maximum energy transfer between the incoming gamma-ray and the electron.

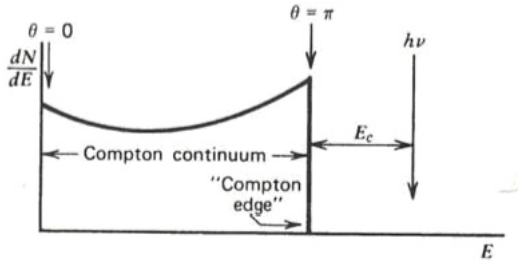

Figure 3.4: A sketch of the Compton continuum.

In the detector, all scattering angles from 0 to π will occur. Because of this, a continuum of energies can be transferred to the electron. This continuum can be seen in Figure 3.4. This energy has a range from 0 all the way to the maximum predicted by Equation 1. Figure 3.5 shows that for any one specific gamma-ray energy, the electron energy distribution has the general shape shown in the figure.

The energy of the incident photon after backscattering is given by

$$h\nu' \mid_{\theta=\pi} \quad = \quad \frac{h\nu}{1 + 2h\nu/m_0c^2} \tag{2}$$

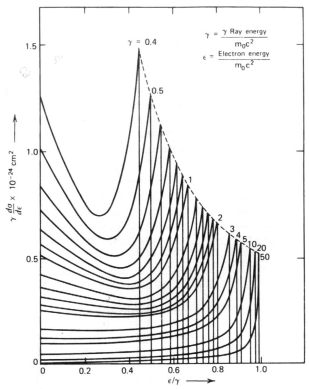

Figure 3.5: Shape of the Compon continuum for various gamma-ray energies.

The gap between the maximum recoil electron energy and the actual energy of the incident photon is given by

$$E_C \equiv h\nu - E_{e^-}|_{\theta=\pi} \quad = \quad \frac{h\nu}{1 + 2h\nu/m_0c^2} \tag{3}$$

In actual detectors, the binding energy of electrons will actually alter the shape of the Compton continuum. The Compton continuum will be observed at the lower energy end of the spectrum.

3.1.3 Pair Production

Pair production is a gamma-ray that turns into an electron-positron pair. This occurs when the gamma-ray is in the intense electric field near the nuclei of the absorbing material. There is a minimum amount of gamma-ray energy that is required for this process to take place. This minimum energy is the mass of the electron-positron pair, $2m_0c^2$. Therefore, the conservation of kinetic energies gives

$$E_{e^-} + E_{e^+} \quad = \quad h\nu - 2m_0c^2 \tag{4}$$

The plot of the total kinetic energy created by the incident gamma-ray is a delta function that is shift a distance of $2m_0c^2$ away from the incident photon energy, $h\nu$. The position of this energy is called the *double escape peak* in an actual gamma-ray pulse height spectra. This is a very complicated process due to the fact that a positron is not stable. It will annihilate when it comes into contact with an electron, which are very abundant. Upon annihilation, two 0.511 MeV photons will be released back into the system. This process will happen quite quickly and will appear to be in coincidence with the original pair production. In some cases, only one of the annihilation photons is absorbed inside the detector. This produces a peak that is known as the *single escape peak* on the pulse-height spectrum.

3.2 Detector Response Function

Imagine a detector that was much larger than the mean free path of the fast electrons that are created by a gamma-ray interaction in the medium of the detector from a gamma source that emits mono-energetic photons.

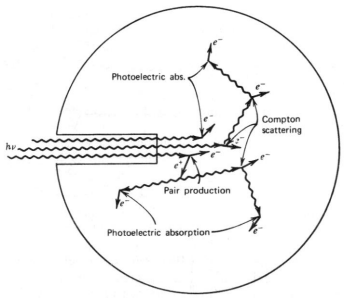

Figure 3.6: A detector that is large enough such that all gamma-ray interactions are absorbed within the detector.

Figure 3.6 is a diagram of such a detector. It can be seen that all of the gamma-ray interactions are absorbed by the detector.

Under these ideal conditions, the spectrum will take the form of a figure that was mentioned earlier in the text, Figure 3.3. The large peak that is labeled full-energy peak, is often known as the *photopeak* in detectors that do not absorb all of the gamma-ray energy.

Unfortunately, gamma-rays often carry a lot of energy and building a detector large enough to stop all of them from escaping isn't always practical and sometimes just isn't feasible.

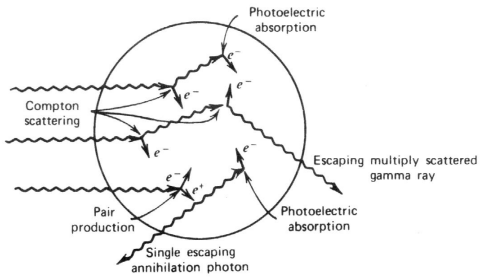

Figure 3.7: Gamma-ray interactions with a detector of average size.

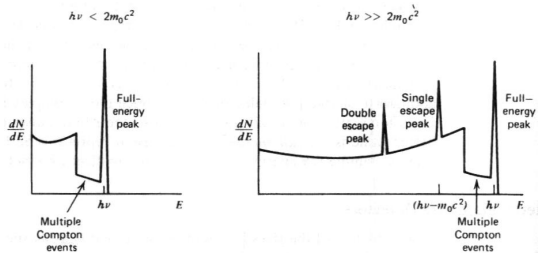

Figure 3.8: The pulse-height spectra of an average-sized detector.

Figure 3.7 shows the gamma-ray interactions inside a more realistic detector. Figure 3.8 is a sketch of the pulse-height spectrum for such a detector. It can be seen that the energy of the photon is no longer a distinct peak, but has a whole spectrum of energies. This spectrum

of energies depends on many factors. The size, shape, geometry, and composition of the detector are all factors that attribute to the shape of the pulse-height spectrum. A couple of spectrum properties that are often quoted are the *photofraction*, the ratio of the area under the photopeak to the area under the entire spectrum, and the ratio of the area under a single or double escape peak to the area under the photopeak.

3.3 Complications in the Response Function

Unfortunately, there are several factors that complicate the spectrum even further that we must consider. These factors are: secondary electron escape, Bremsstrahlung escape, characteristic X-ray escape, secondary radiations created near the source, the effects of surrounding materials, and coincidence.

3.3.1 Secondary Electron Escape

For high energy gamma-rays, the resulting secondary electrons (the electrons created by a gamma-ray interaction) will also have high energy. These high energy particles have a high probability of penetrating the detector and leaking out of the system. This effect will also be prevalent in detectors that are too small for the system they are observing. This electron leakage will distort the response function. The Compton continuum along with other low amplitude energies will be shifted to favor lower amplitudes. Since events are escaping the system, the photopeak will be reduced as well. This loss of events from the photopeak will also reduce the photofraction.

3.3.2 Bremsstrahlung Escape

Bremsstrahlung photons are electromagnetic radiation that is emitted from the decelerating, charged particle. In this case, that charged particle is an electron that is being decelerated by scattering off of other nuclei. This causes a problem when the bremsstrahlung photons are emitted and not reabsorbed by the detector. Production of bremsstrahlung photons is proportional to Z^2 of the absorber. This alters the response function in the same manner that the escape of secondary electrons alters the response function. The effects of bremsstrahlung can be minimized by using materials with low atomic numbers.

3.3.3 Characteristic X-Ray Escape

As described in the photoelectric absorption process, a characteristic X-ray is released by an absorber atom that is, in most cases, reabsorbed near the atom that emitted it. If this process takes place near the surface of a detector, the characteristic X-ray may escape the detector and alter the response function, as Figure 3.9 shows.

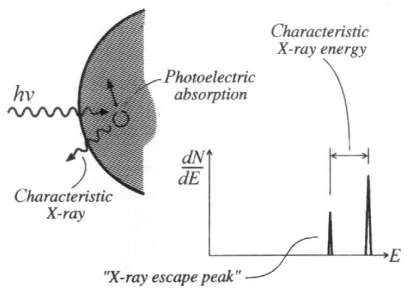

Figure 3.9: A characteristic X-ray escaping a detector and the effect it has on the response function.

By escaping, the characteristic X-ray creates a new peak in the response function. This peak appears a distance of the characteristic X-ray energy away from the photopeak and is known as the *X-ray escape peak*. This phenomena is prevalent in low energy incident photons and detectors with a large surface-to-volume ratio.

3.3.4 Secondary Radiations Created Near the Source

Secondary radiations are the radiations that are emitted by particles that are emitted from the source, as in β^- and β^+ decay, and make it to the detector. In other words, they are radiation events that are caused by the source instead of emitted from the source. In β^--decay, the electrons do not usually make it to the detector, but they give off bremsstrahlung radiation that will penetrate and interact inside of the detector. For β^+-decay, the photon emitted upon annihilation of the positron can also enter the detector and alter the response function.

Both of these types of secondary radiations will increase the overall energy that is detected in the system. These secondary radiation energies will be superimposed onto the response function. The result in this is a shift of the spectrum to favor higher amplitudes.

3.3.5 Effects of Surrounding Materials

Often, the gamma-rays emitted from a source will not interact within the detector, but will interact with the materials that house the detector or any other surround material. It is not uncommon for the results of these interactions to then be absorbed by the detector.

Figure 3.10 depicts the creation of radiation from material surrounding the detector and then effect that they have on the response function. In Figure 3.10, event (1) represents X-ray events. This additional peak in the response function is a result of the detector absorbing the characteristic X-rays that are emitted from the surrounding materials. Event (2) corresponds to the backscattering. This is a wider peak because of the broad range of energies a backscattered photon can have. However, due to the energetics of the backscattering process, the backscattering peak always occurs at energies of 0.25 MeV or less. Event (3)

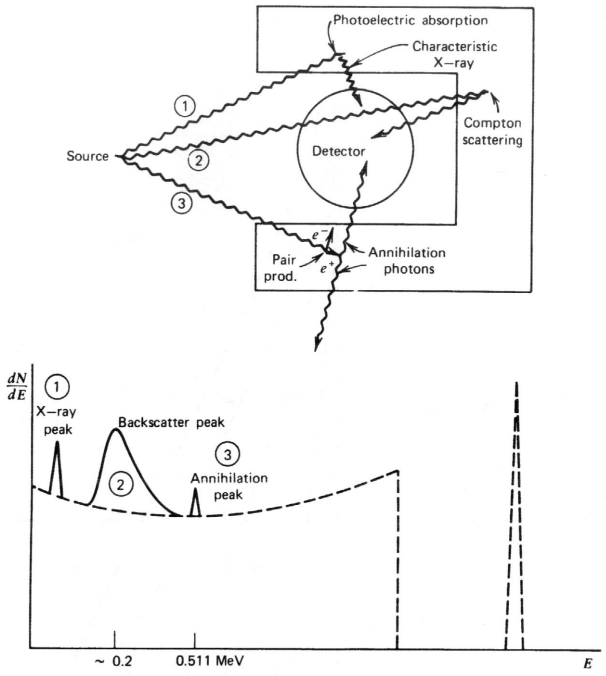

Figure 3.10: Influence of surrounding materials on detector response. In addition to the expected spectrum (show as a dashed line), the representative histories shown at the top lead to the indicated corresponding features in the response function.

is the creation of foreign annihilation photons. This will always cause a significant boost to the response function at 0.511 MeV. This significant yield of annihilation radiation is only a concern in systems surrounded by high-Z materials.

3.3.6 Summation Peaks

Summation peaks occur when two gamma-rays are emitted in quick succession, such that they appear to emitted instantaneously. This seemingly instantaneous emission of separate gamma-rays is known as coincidence. In this situation, the detector will see both of those energies as one larger energy deposited in the detector. The result of this is a peak on the spectrum that is larger than any characteristic gamma-ray that a source gives off. A tell-tale sign of a summation peak is a prominent peak that has the same energy as two characteristic

gamma-rays of the source.

3.4 Semiconductor Diode Detectors

The processes that take place within the semiconductor allowing it to be a useful radiation detector are plentiful and an entire report could be spend discussing this vast topic. All that will be discussed here is why semiconductors are used over scintillators or other types of detectors and the basics of how they work.

Scintillation counters have very poor radiation resolutions due to the fact that the process of converting an incident radiation to light and then to an electrical signal is not only long, but it is inefficient as well. Semiconductors do not have to suffer through this laborious process, and therefore their resolution is much higher.

The periodic lattice of crystalline materials establishes allowed energy bands for electrons that exist within a solid. The energy of any electron inside a pure material must be confined to one of these bands. Certain energies are forbidden, and these are visualized as gaps. There are two types of bands that are of interest: the valence band and the conduction band. The lower band, known as the valence band, corresponds to outer-shell electrons that are bound to specific lattice sites within the crystal. The next higher-lying band is known as the conduction band and represents electrons that are free to migrate through the crystal. If an electron lies within the conduction band then it contributes to the overall electrical conductivity of the material. The gap between these bands is known as the bandgap. The bandgap for a semiconductor is less than the dielectric for that material. The size of this gap is quoted as an energy, E_g. Figure 3.11 diagramatically depicts this bandgap.

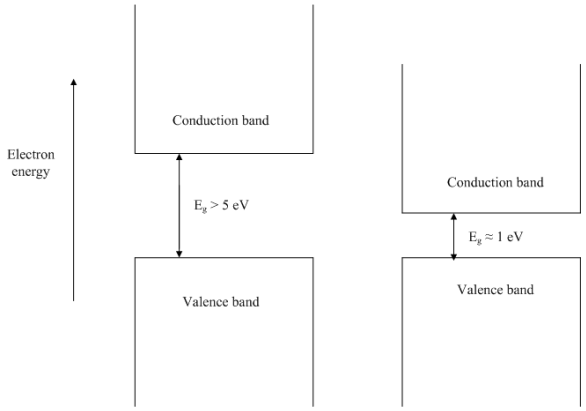

Figure 3.11: Band structure for electron energies in insulators and semiconductors.

If an electron gains an energy of E_g or greater, than it will gain the ability to jump up into the conduction band and then lend itself to electrical conductivity. In a semiconductor, the value for E_g is less than the dielectric for that material.

The excitation of an electron process not only creates an electron in the conduction band, but it also leaves a hole in the valence band. The combination of these two is known as an *electron-hole pair*. It is analogous to the ion pairs created inside the gas-filled detector in the fact that they are what is used to carry charge.

The probability per unit time that an electron-hole pair is thermally generated is given by

$$p(T) \quad = \quad CT^{3/2}\exp\left(-\frac{E_g}{2kT}\right) \tag{5}$$

where T = absolute temperature, E_g = bandgap energy, k = Boltzmann constant, and C = proportionality constant characteristic of the material.

As reflected by Eq. 5, the probability that an electron will jump to the conduction band is very sensitive to temperature. Often being at room temperature will supply electrons with enough energy to jump into the conduction band in many materials. Because of this, semiconductors with small bandgaps need to be severely cooled in order to be of use in detection. The smaller the bandgap of a semiconductor is, the better that semiconductor is at discriminating very small differences in energies. In other words, a small bandgap leads to a high resolution detector.

Creating the electron-hole pairs is the mechanism by which the semiconductor detects radiation. When a charged particle passes through a semiconductor, electron-hole pairs are created along the path of the charged particle. These electrons allow for the conduction of electricity. In short, this conduction of electricity allows a pulse to be formed. The larger the energy of the incident particle, the more electron-hole pairs are formed, and thus a higher pulse is the result.

3.5 High Purity Germanium Semiconductor Detectors

High purity germanium, or simply HPGe, detectors are semiconductor detector crystals that are manufactured from ultrapure germanium. The reason that high level of purity in the material is desired has to do with the depletion region. The depletion region is desired to be as large as possible. The depletion equation is

$$d = \left(\frac{\epsilon V}{eN}\right)^{1/2} \tag{6}$$

where e is the electronic charge, ϵ is the dielectric constant, V is the reverse bias voltage, and N is the net impurity concentration in the bulk semiconductor material. As it follows from the

Eq. 6, the lower the impurity concentration, the higher the depletion depth is. Germanium is chosen for the reason that current manufacturing techniques allow for germanium to be refined such that the purity concentration is as low as 10^{10} atoms/cm^2. At this level of impurity, a depletion depth of 10 mm can be obtained with a reverse bias voltage of less than 1000V.

3.5.1 HPGe Geometry

It is ideal for a detector like this to maximize volume in order to absorb as many gamma-rays as possible. In order to do this, our detector has as coaxial geometry as shows in Figure 3.12.

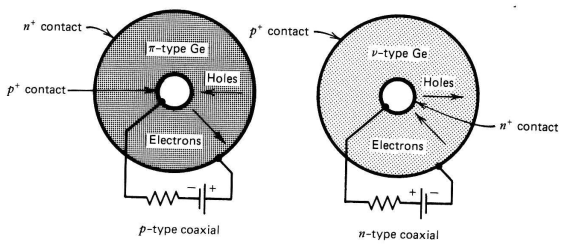

Figure 3.12: Cross sections perpendicular to the cylindrical axis of the detector crystal.

There are electrodes connected to contact on the inside of the coaxial and the outside of the coaxial. A potential is applied across the coaxial and a potential is applied across the detector. Due to the geometry of the detector, electron-hole pairs have to travel different distances to get to the electrodes, depending on where they were created. Because this collection time is not constant, the pulse shape is also not constant as well.

3.6 Germanium Detector Setup

Due to the small bandgap of about 0.7 eV, germanium detectors are impossible to operate at room-temperature. This lack of functionality at room-temperature stems from the large thermally-induced leakage current that results at this temperature. In order to get around

this, the germanium detector is cooled to the point where this thermal leakage no longer spoils the excellent energy detections. This temperature happens to be 77 K and is achieved through the use of liquid nitrogen to cool the detector.

The detector requires constant cooling from the liquid nitrogen in order to maintain the great energy resolution that it has. A special apparatus has been constructed to aid in that task. Appendix H has a sketch of such a device. The detector must be housed in a vacuum-tight cryostat to inhibit thermal conductivity between the detector crystal and the surrounding air. The cryostat is just capsule that houses the germanium crystal. A thin window is usually located near the crystal to minimize attenuation of gamma rays before they enter the germanium. As it is shown in Appendix H, the cryostat is mounted on a liquid nitrogen dewer. The dewer houses all of the liquid nitrogen and allows the germanium crystal to maintain its low temperature. The dewer must be much larger than the detector crystal itself in order to maintain liquid nitrogen for periods of time such that the dewer does not need constant filling.

3.7 Energy Resolution

The great advantage to using a germanium detector is the fact that they have excellent energy resolution for gamma-ray spectroscopy. A high energy resolution means that the detector can discriminate between gamma-rays with similar energies. The more resolution a detector has, the more defined a gamma spectrum becomes. Recall that the resolution of a detector is defined as

$$R = \frac{H_0}{\text{FWHM}} \tag{7}$$

where H_0 is the centroid peak number and FWHM is the full-width half-maximum of the peak.

There are three factors that give germanium the excellent resolution that it has: the inherent statistical spread in the number of charge carriers, variations in the charge collection efficiency, and contributions of electronic noise. Some of these factors will dominate over the other factors, but this is dependent on the energy of the radiation and the size and quality of the detector in use.

3.8 Background Radiation

It is of importance to analyze the background spectrum due to the cosmic radiation that constantly bombards the planet as well as the radiation that is ambient due to the natural radioactivity of the environment. There are five categories that background radiations are classified as:

1. The natural radioactivity of the constituent materials of the detector itself.
2. The natural radioactivity of the ancillary equipment, supports, and shielding placed in the immediate vicinity of the detector.
3. Radiations from the activity of the earth's surface (*terrestrial radiation*), construction materials of the laboratory, or other far-away structures.
4. Radioactivity in the air surrounding the detector.
5. The primary and secondary components of cosmic radiation.

The most significant sources for background radiations are ^{232}Th, ^{238}U, and ^{40}K. ^{40}K is a significant source because it has a half-life that is larger than the age of the earth. ^{232}Th and

^{238}U are significant contributors to the background radiation because of their abundance in many materials as well as the long decay chains that they produce. In these decay chains, all different types of radiation at a large range of energies are emitted.

Cosmic radiation also contributes to background radiation. The planet is constantly bombarded with high energy particles such as muons, pions, neutrons, electrons, positrons, etc. They particles have low energy loss rates and therefore can be significant contributors to background radiations. The high energies can produce large pulse heights in a spectrum and give false readings for a source that is being measured.

4 Equipment List

The following equipment was used in the laboratory:

- Ortec 459 Bias Supply
- Ortec 572 Amplifier
- Dell OptiPlex GX100 running Maestro
- RG58u Polyethylene Coaxial Cable

5 Setup & Settings

One setup was used throughout the entire course of this lab. The detector was connected to an amplifier and a bias supply in the NIM BIN via coaxial cable. The NIM BIN was then connected to a computer running Maestro via coaxial cable. Figure 5.1 shows what this setup looks like.

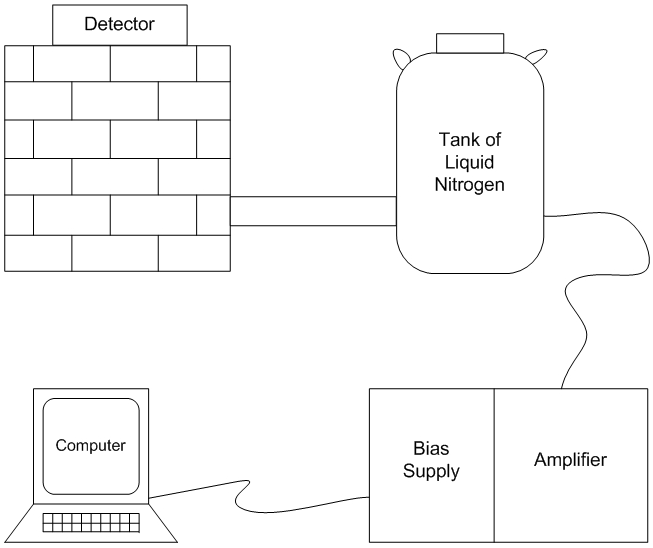

Figure 5.1: The equipment diagram for the gamma ray spectroscopy experiment.

The settings for the bias supply were as follows:

- Negative Polarity
- -3000 V

The settings for the amplifier were as follows:

- Fine Gain = 1.1
- Coarse Gain = 200
- Shaping Time = 1 μs
- Unipolar
- Negative Polarity

After dialing in the appropriate equipment settings, a 15 min background count was taken using Maestro. After doing this, a source was placed on the detector. The purpose of this

next reading is to calibrate the MCA so that each channel would correspond to an energy. The sources were long, clear rods with a black tip at the end. The black tip housed the radioactive source. This part was placed in the middle of the detector to minimize error due to the solid angle of the measurements. The sources were placed a distance away from the crystal that should have effectively reduced any error due to dead time of the system. After placing the first source, ^{22}Na, on the detector, a measurement was made with the MCA. The measurement was taken until there were at least 1000 counts. Using a chart of isotopes, two major gamma energies were identified and entered into the auto-calibrate function that Maestro has. After calibrating the MCA, measurements for each of the different isotopes were able to be accurately made. After each measurement, the spectrum was moved to the buffer and the background count was subtracted from it and then saved. After doing this for the following isotopes,

$$^{57}\text{Co},\ ^{60}\text{Co},\ ^{137}\text{Cs},\ ^{22}\text{Na},\ ^{133}\text{Ba},\ ^{109}\text{Cd},\ ^{54}\text{Mn}$$

the data was ready to be analyzed.

6 Analysis

A 12-bit MCA was used to record the spectra, thus there were 4096 channels available for measurement. The centroid channel number for all prominent peaks as well as the channel number location of all other interesting features were recorded. The FWHM (in channels), area under each photopeak, and the area under the spectrum was also recorded, as was instructed by part 4 of the lab instructions.

A majority of the spectra that were gathered in lab were of very poor quality. It is possible that the count times were too low to build up a decent spectrum. Also, the background

spectrum consists of about 16 total counts. A hypothesis for this is that while recording the spectra, some erroneous data was saved to the file name of the background spectra. The low quality background count made subtracting this spectrum from the other spectra meaningless. This will also provide later complications in analyzing the background spectrum.

6.1 Prominent Peak Information

Table 1 displays the information required by part 4 of the lab instructions:

6.2 Calibration Curve

In part 5 of the lab instructions, a plot of the peak energy vs. channel number is required. This curve is the energy calibration curve, and can be seen in Figure 6.1.
There are a couple of things that are of note in Figure 6.1. First, is the R^2 of the best fit line. It has a value of 1, meaning that the best fit line is a perfect match for the data. This is an excellent result. The second thing of note, is the actual best fit line itself. The equation for this line is

$$\text{Energy (keV)} = 0.9845 * \text{Channel Number} + 2.003 \quad (8)$$

The implication of this equation is that for any given channel on the MCA, by plugging that channel number into Eq. 8, the energy that the MCA channel represents can be calculated. This means that the MCA is linear; each channel has the same width of energy. Part 6 of the lab instructions asks for the following criteria to be labeled on all prominent features on

Channel Number	Energy (keV)	FWHM	Gross Area	Total Spectrum Area
^{57}Co Source				
76	74.41	2.78	512	3592
123	122.65	2.78	119	3592
^{60}Co Source				
1157	1154.03	2.29	677	10648
1314	1310.54	2.25	561	10648
1439	1436.92	1.00	15	10648
^{137}Cs Source				
34	33.40	1.99	1854	18667
76	75.51	1.14	858	18667
653	653.28	1.91	3037	18667
^{22}Na Source				
76	89.16	3.87	342	6159
505	520.30	2.85	903	6159
1257	1274.60	2.52	222	6159
^{133}Ba Source				
32	32.16	1.86	43007	98873
54	54.08	0.97	3882	98873
82	81.26	1.81	19253	98873
274	272.82	1.79	1804	98873
300	298.72	1.78	3148	98873
352	350.89	1.60	7833	98873
379	378.29	1.81	1106	98873
^{109}Cd Source				
37	44.66	1.34	2351	359510
88	88.19	1.70	34709	359510
^{54}Mn Source				
76	74.98	2.91	5106	92322
824	821.71	2.02	13920	92322

Table 1: Peak information for all interesting features on the gamma-ray spectra recorded in lab.

the gamma spectra for each source: channel number, calculated/expected energy, measured energy, and the percent difference between expected and measured energy.

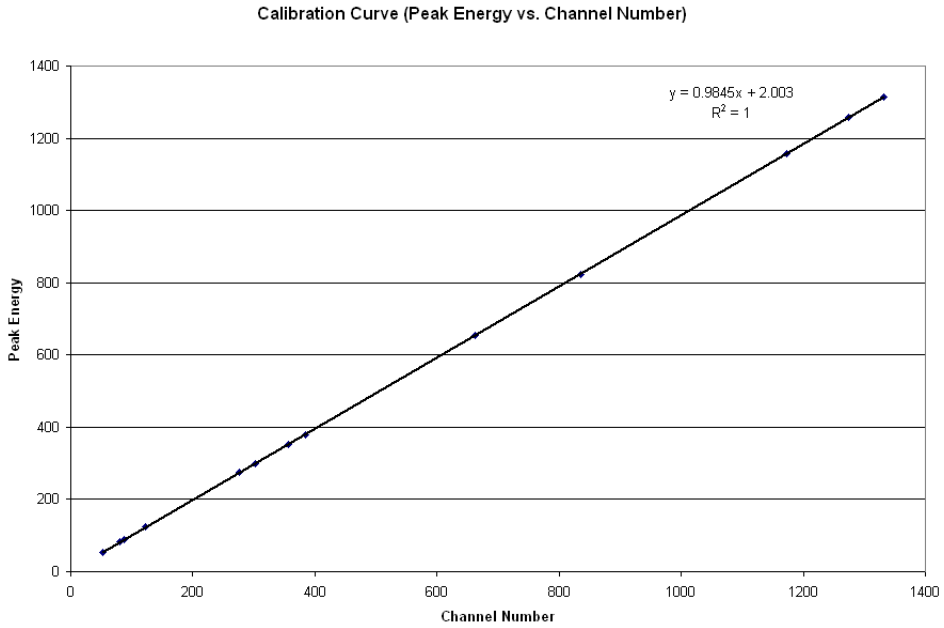

Figure 6.1: The calibration curve for the germanium gamma-ray detector.

6.3 Experiment Part 6 – ^{57}Co

For ^{57}Co, the spectrum in Figure 6.2 is produced. This spectrum looks distorted, but there still are prominent features that are identifiable. Table 2 organizes the information of the peaks that were identified on the spectrum.

^{57}Co Source				
Spectrum Feature	Channel Number	Measured Energy	Expected Energy	% Difference
Pb $K_{\alpha 1}$	77	77.810	74.969	3.79
Pb $K_{\beta 1}$	86	86.67	84.94	2.04
Photopeak	122	122.11	122.06	0.0426

Table 2: Peak information for prominent features on the ^{57}Co spectrum.

The Pb $K_{\alpha 1}$ and Pb $K_{\beta 1}$ are X-rays that are characteristic of lead. The bricks that contain the germanium detector are made of lead. Therefore, we can conclude that these X-rays are

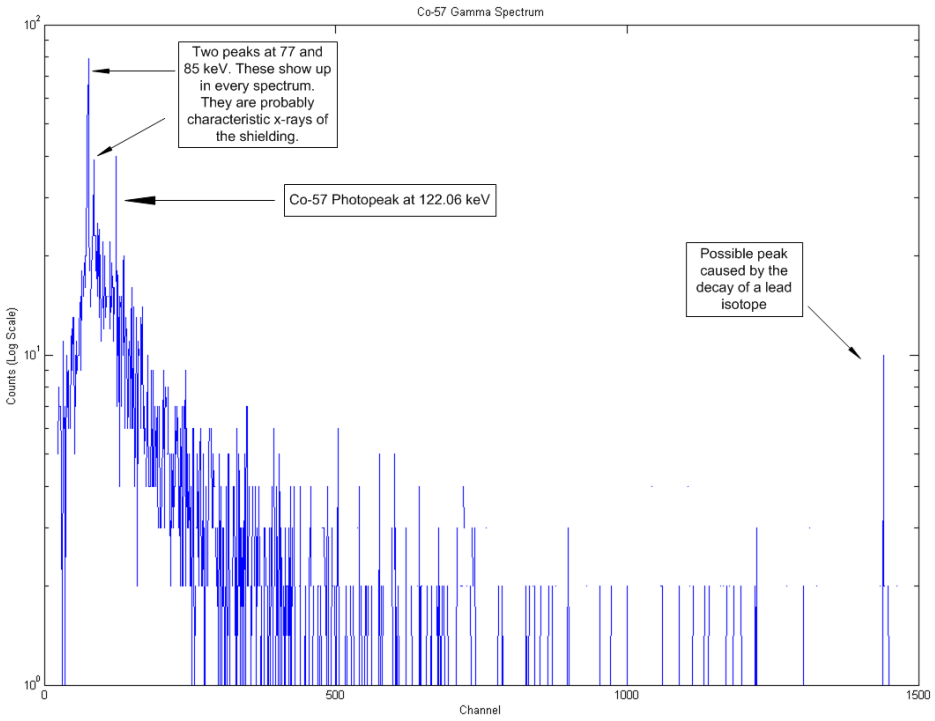

Figure 6.2: The ^{57}Co gamma spectrum with select features labeled.

being emitted from the lead bricks around the detector and that we can expect to see them in every spectrum. It should be noted that the errors between the measurement and the actual value of the X-rays are very small. We can expect a relatively small error (2 - 3%) due to the fact that we are using a 12-bit MCA that gives us 4096 channels. This error could be reduced even further with more MCA channels. The photopeak was detected right where we would expect it be, at 122.1 keV. The error between the measured and the actual here is almost nonexistent[1]. It should be noted that there are no single escape, double escape, or annihilation peaks on this spectrum. This is exactly what is expected, as the gamma-rays emitted by this source are not energetic enough (1.022 MeV) to undergo pair production.

[1]All error percentages were taken to be positive.

6.4 Experiment Part 6 – ^{60}Co

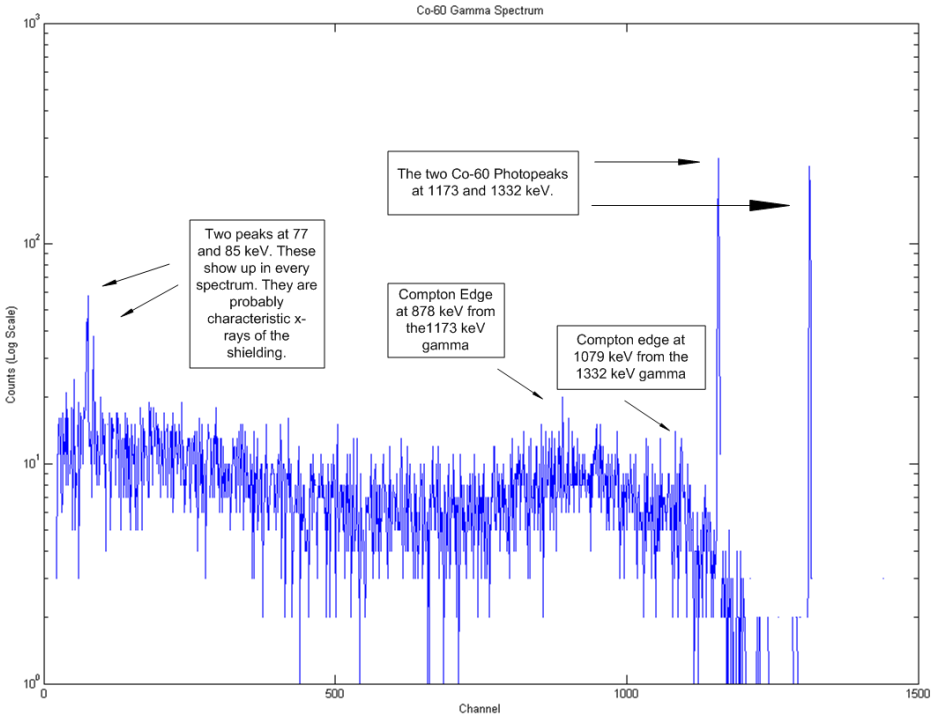

Figure 6.3: The ^{60}Co gamma spectrum with select features labeled.

For ^{60}Co, the spectrum in Figure 6.3 is produced. This spectrum is also distorted, although the features are more distinguishable than the those on the ^{57}Co spectrum. Table 3 organizes the information of the peaks that were identified on the spectrum.

Again, the Pb $K_{\alpha 1}$ and Pb $K_{\beta 1}$ are X-rays that are characteristic to lead show up as expected. The next two noteworthy features on the spectrum (Figure 6.3) are the two photopeaks. ^{60}Co produces two distinct gammas: one at 1173 keV and one at 1332 keV. These peaks show up right where they are expected and there is good agreement between the measurement and the actual energies (within 3%).

^{60}Co Source				
Spectrum Feature	Channel Number	Measured Energy	Expected Energy	% Difference
Pb $K_{\alpha 1}$	77	77.810	74.969	3.79
Pb $K_{\beta 1}$	86	86.67	84.94	2.04
Photopeak 1	1158	1142.1	1173	2.64
Photopeak 2	1315	1296.6	1332	2.66
Compton Edge 1	890	878.2	948.7	7.43
Compton Edge 2	1094	1079.0	1101	1.99

Table 3: Peak information for prominent features on the ^{60}Co spectrum.

It is here that an interesting phenomenon occurs. Each of the two gammas will create their own Compton continuum on the spectrum. These continuum overlap, but the Compton edges are still distinctly visible for each region. These Compton edges are labeled on Figure 6.3. Using Eq. 3, the Compton edge energy is able to be calculated. The error between these calculations and the measurements taken in the lab were surprisingly small. The spectrum is too rough to really see any definition in the regions where we might expect to see single escape, double escape, or annihilation peaks. This is not what is expected, as the gamma-rays emitted by this source are energetic enough (1.022 MeV or greater) to undergo pair production. We can assume that the spectrum is not defined enough for these features to be visible and that another count should be taken more carefully in order to find those features.

6.5 Experiment Part 6 – ^{137}Cs

For ^{137}Cs, the spectrum in Figure 6.4 is produced. Table 4 organizes the information of the peaks that were identified on the spectrum.

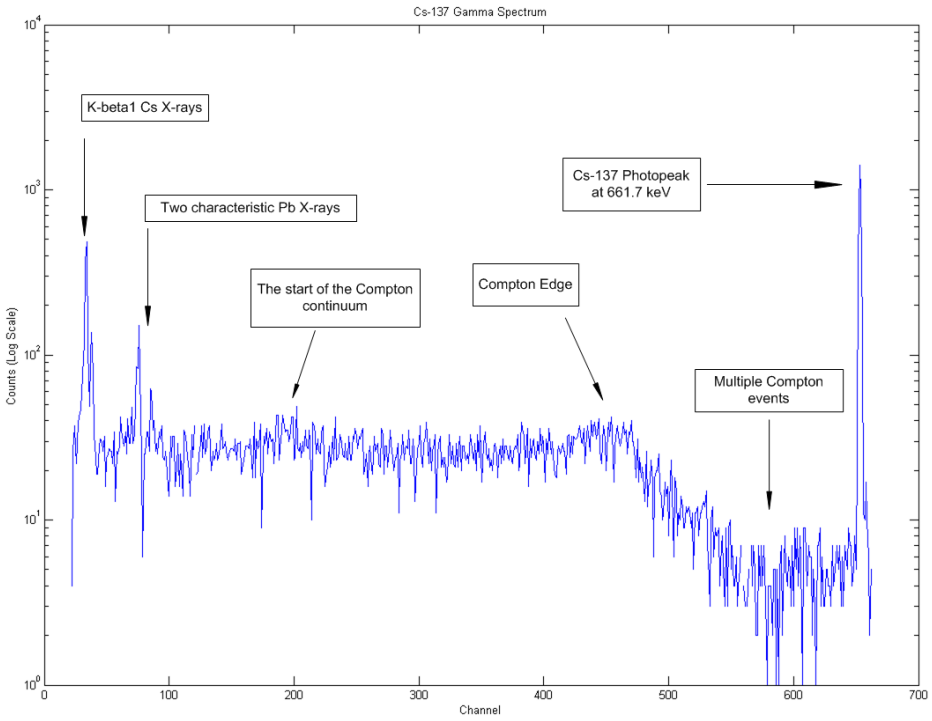

Figure 6.4: The ^{137}Cs gamma spectrum with select features labeled.

Spectrum Feature	Channel Number	Measured Energy	Expected Energy	% Difference
Cs $K_{\beta 1}$	34	35.476	34.987	1.40
Cs $K_{\beta 4}$	38	39.414	35.907	9.77
Pb $K_{\alpha 1}$	77	77.810	74.969	3.79
Pb $K_{\beta 1}$	86	86.67	84.94	2.04
Compton Start	187	186.105	183.65	1.34
Compton Edge	470	464.718	469.355	0.988
Photopeak	653	644.88	661.7	2.54

Table 4: Peak information for prominent features on the ^{137}Cs spectrum.

Again, the Pb $K_{\alpha 1}$ and Pb $K_{\beta 1}$ are X-rays that are characteristic to lead show up as expected. The next two noteworthy features are first two items on the table. They are the characteristic X-rays of Cs. They show up through the photoelectric absorption process that is outlined in Section 3.1.1. Using Eqs. 2 and 3 we can calculate the location that we expect to see the

beginning and the end of the Compton continuum. When compared to the measurements made in the laboratory, there is excellent agreement between these values (within 2% error). ^{137}Cs emits one gamma-ray at 661.7 keV. This peak is easily identifiable on the spectrum. The measured peak comes within 2.54% of the actual energy. It should be noted that there are no single escape, double escape, or annihilation peaks on this spectrum. This is exactly what is expected, as the gamma-rays emitted by this source are not energetic enough (1.022 MeV) to undergo pair production.

6.6 Experiment Part 6 – ^{22}Na

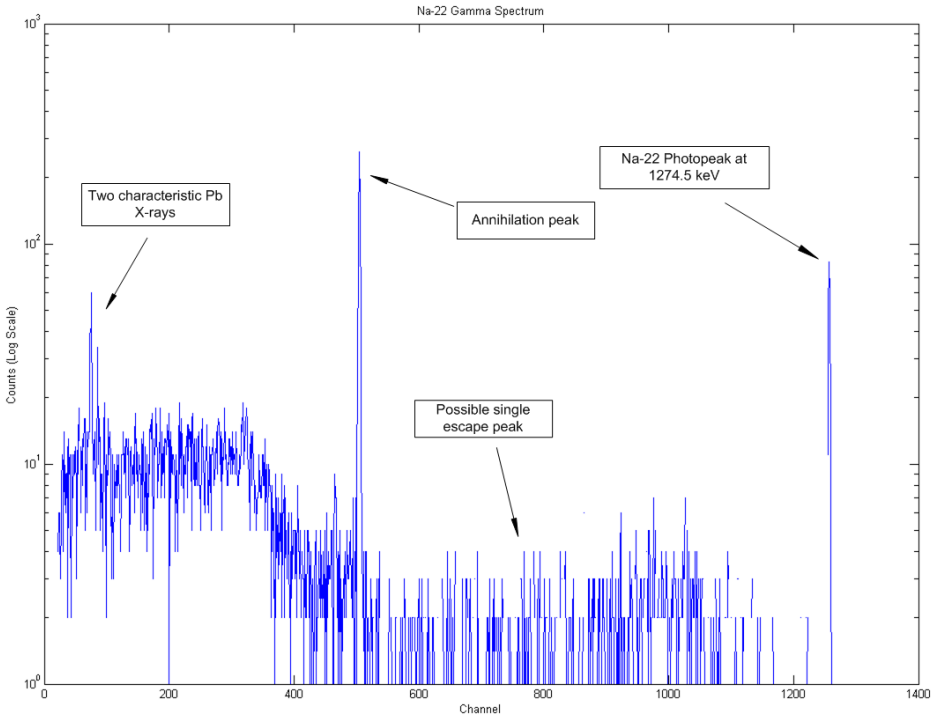

Figure 6.5: The ^{22}Na gamma spectrum with select features labeled.

For ^{22}Na, the spectrum in Figure 6.5 is produced. Table 5 organizes the information of the

peaks that were identified on the spectrum.

Spectrum Feature	Channel Number	Measured Energy	Expected Energy	% Difference
Pb $K_{\alpha 1}$	77	77.810	74.969	3.79
Pb $K_{\beta 1}$	86	86.67	84.94	2.04
Annihilation	504	498.2	511	2.51
Single Escape	763	753.2	763.5	1.35
Photopeak	1257	1239.5	1274.5	2.74

Table 5: Peak information for prominent features on the ^{22}Na spectrum.

Again, the Pb $K_{\alpha 1}$ and Pb $K_{\beta 1}$ are X-rays that are characteristic to lead show up as expected. ^{22}Na proves to be an interesting source because its gamma-decay energy is 1274.5 keV. Because of this energy, it is energetically possible for pair production to occur. As a directly result of the ^{22}Na source causing pair production, a sharp peak is produced at 511 keV. This peak is know as the annihilation peak and its creation is detailed in Section 3.1.3. There is good agreement between the experiment and theory on that measurement. The photopeak measured at 1274.5 keV also shows good agreement with theory. There appears to be a slight peak at 735.2 keV. This is a value of about 511 keV away from the photopeak. This type of peak is known as the single escape peak and is formed when one of the β-particles made in pair production escapes the detector. There appears to be a Compton continuum in the spectrum but it is too distorted to be sure. Another spectrum would have to be measured to verify this hypothesis.

6.7 Experiment Part 6 – ^{133}Ba

For ^{133}Ba, the spectrum in Figure 6.6 is produced. Table 6 organizes the information of the peaks that were identified on the spectrum.

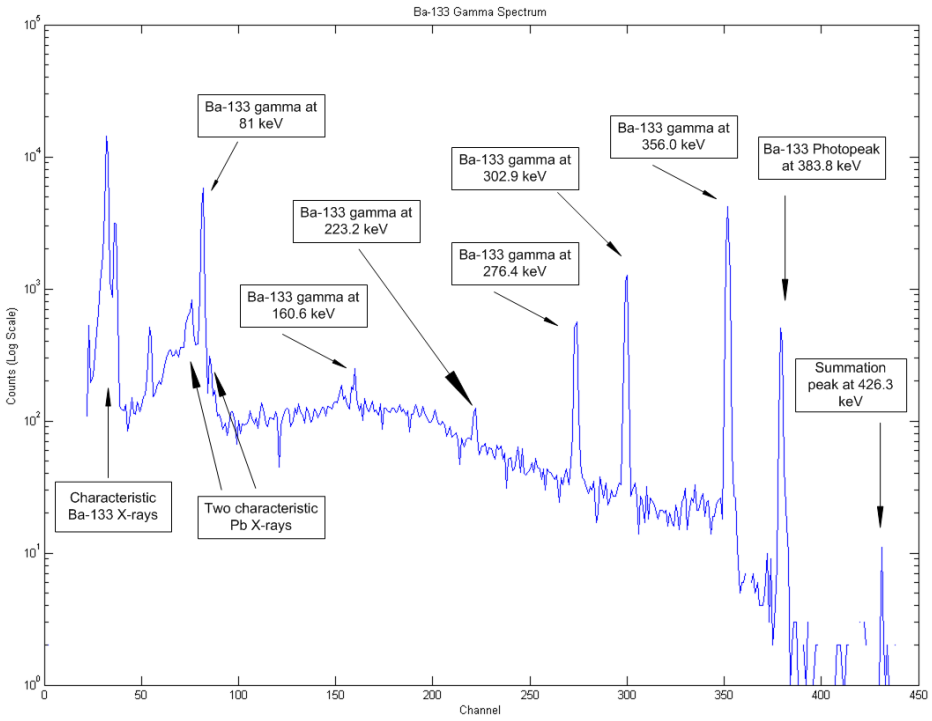

Figure 6.6: The ^{133}Ba gamma spectrum with select features labeled.

Spectrum Feature	Channel Number	Measured Energy	Expected Energy	% Difference
Ba $K_{\alpha 1}$	32	33.51	32.194	4.08
Ba $K_{\beta 1}$	36	37.45	36.48	2.93
Pb $K_{\alpha 1}$	77	77.810	74.969	3.79
Pb $K_{\beta 1}$	86	86.67	84.94	2.04
Peak 1	83	83.7	81.0	3.35
Peak 2	160	159.523	160.61	0.678
Peak 3	222	220.5	223.2	1.20
Peak 4	274	271.8	276.4	1.68
Peak 5	300	297.4	302.9	1.82
Peak 6	352	348.5	356.0	2.10
Peak 7	379	375.1	383.8	2.27
Summation Peak	431	426.3	–	–

Table 6: Peak information for prominent features on the ^{133}Ba spectrum.

Again, the Pb $K_{\alpha 1}$ and Pb $K_{\beta 1}$ are X-rays that are characteristic to lead show up as expected. The first two features on Table 6 are the characteristic X-rays from Ba. They show up from the photoelectric absorption process that is outlined in Section 3.1.1. ^{133}Ba is a source that emits many different gamma-rays. This can be seen on the gamma spectrum. After matching all of the gamma energies in the table of isotopes with the gammas that were measure, all of their agreements with actual values were tabulated. The last item on the table is a summation peak. It's energy of 426.3 keV comes from the cascade emission of the 356 keV and 81 keV gamma-rays. No Compton continuum values were calculated because each of the emitted gammas creates its own range of Compton values. Thus, with seven peaks, the Compton continuum will be heavily distorted and near impossible to see. It should be noted that there are no single escape, double escape, or annihilation peaks on this spectrum. This is exactly what is expected, as the gamma-rays emitted by this source are not energetic enough (1.022 MeV) to undergo pair production.

6.8 Experiment Part 6 – ^{109}Cd

For ^{109}Cd, the spectrum in Figure 6.7 is produced. Table 7 organizes the information of the peaks that were identified on the spectrum.

^{109}Cd Source				
Spectrum Feature	Channel Number	Measured Energy	Expected Energy	% Difference
Cd $K_{\beta 1}$	24	25.63	26.10	1.78
Cd $K_{\beta 4}$	26	27.60	26.70	3.36
Pb $K_{\alpha 1}$	77	77.810	74.969	3.79
Pb $K_{\beta 1}$	86	86.67	84.94	2.04
Photopeak	88	88.64	88.03	0.687

Table 7: Peak information for prominent features on the ^{109}Cd spectrum.

Again, the Pb $K_{\alpha 1}$ and Pb $K_{\beta 1}$ are X-rays that are characteristic to lead show up as expected.

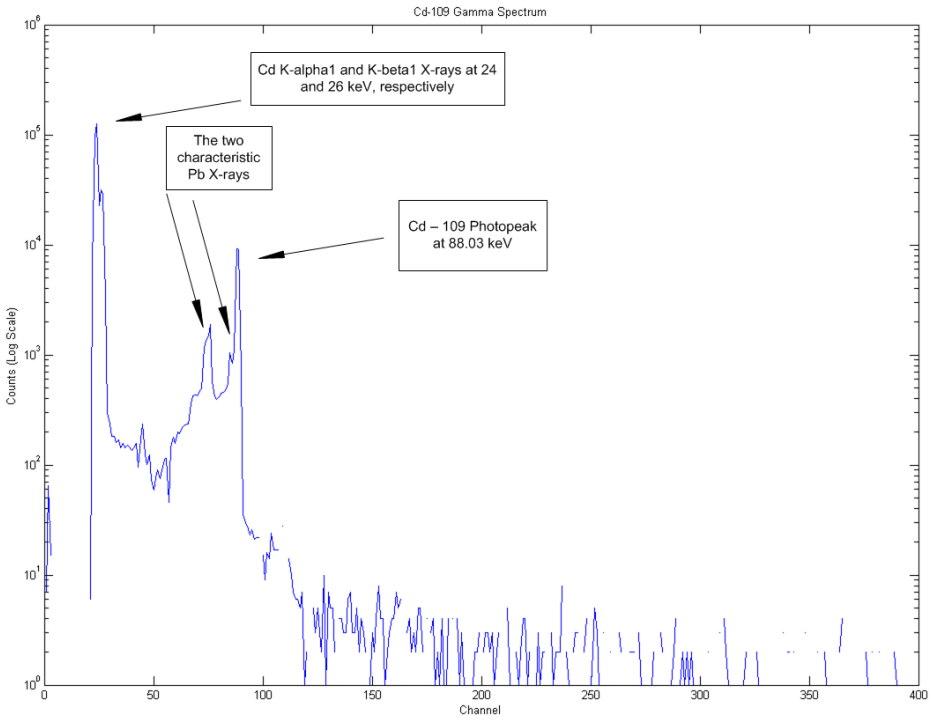

Figure 6.7: The ^{109}Cd gamma spectrum with select features labeled.

The first two features on the table are the characteristic X-rays from Ba. They show up from the photoelectric absorption process that is outlined in Section 3.1.1. The photopeak is located right where it should be and shows excellent agreement with the actual value. It should be noted that there are no single escape, double escape, or annihilation peaks on this spectrum. This is exactly what is expected, as the gamma-rays emitted by this source are not energetic enough (1.022 MeV) to undergo pair production.

6.9 Experiment Part 6 – ^{54}Mn

For ^{54}Mn, the spectrum in Figure 6.8 is produced. This was the best looking spectrum that was recorded in the laboratory for this experiment. Table 8 organizes the information of the

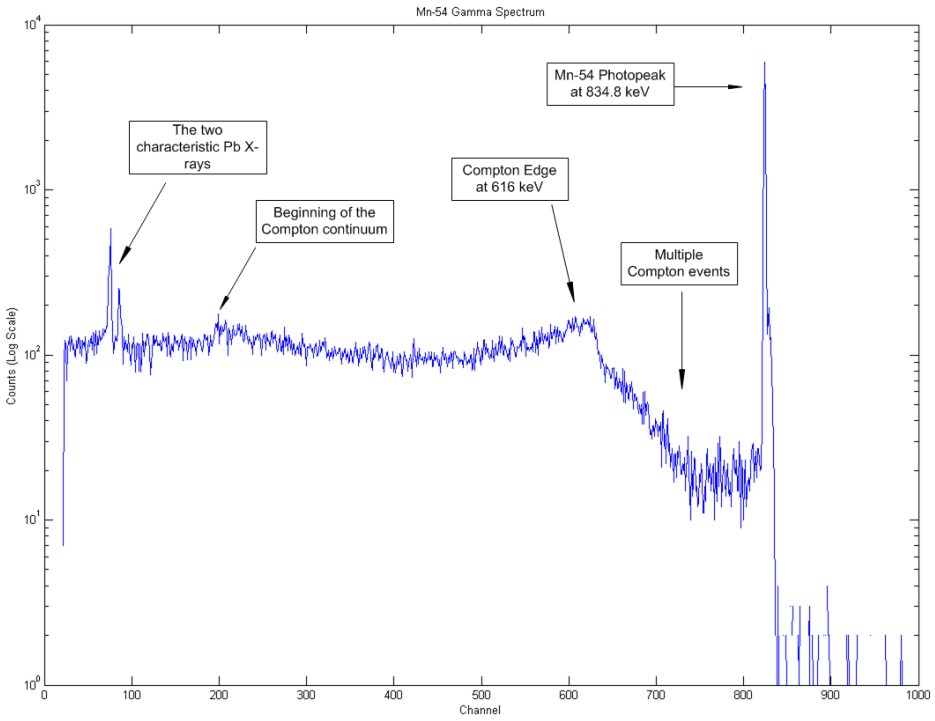

Figure 6.8: The ^{54}Mn gamma spectrum with select features labeled.

peaks that were identified on the spectrum.

^{54}Mn Source				
Spectrum Feature	Channel Number	Measured Energy	Expected Energy	% Difference
Pb $K_{\alpha 1}$	77	77.810	74.969	3.79
Pb $K_{\beta 1}$	86	86.67	84.94	2.04
Compton Start	199	197.92	195.03	1.48
Compton Edge	624	616.33	628.97	2.01
Photopeak	824	813.23	834.8	2.58

Table 8: Peak information for prominent features on the ^{54}Mn spectrum.

Again, the Pb $K_{\alpha 1}$ and Pb $K_{\beta 1}$ are X-rays that are characteristic to lead show up as expected. Using Eqs. 2 and 3 we can calculate the location that we expect to see the beginning

and the end of the Compton continuum. When compared to the measurements made in the laboratory, there is excellent agreement between these values (within 2% error). ^{54}Mn emits one gamma-ray at 834.8 keV. This peak is easily identifiable on the spectrum. The measured peak comes within 2.58% of the actual energy. It should be noted that there are no single escape, double escape, or annihilation peaks on this spectrum. This is exactly what is expected, as the gamma-rays emitted by this source are not energetic enough (1.022 MeV) to undergo pair production.

One thing to note is that the relative amplitudes of the peaks does not have much, if any correlation, with the energy at which they occur at. After observing Figure 6.6, it can be seen that the peaks to the right of the Compton continuum seem to get larger in amplitude leading up to the photopeak and seem to decrease going away from the photopeak. Other than that, no trends are that prevalent.

6.10 Energy Resolution

Part 7 of the lab instructions requires the energy resolution for each observed photopeak. Using the method described in Section 3.7, the energy resolution for each photopeak measured in the lab is calculated. The resolution for each peak was calculated via Eq. 7. This data is organized in Table 9.

Figure 6.9 is the plot of resolution vs. energy on a log-log axis. The slope of this plot represents what the resolution does as energy increases. As Figure 6.9 shows, resolution gets smaller as energy goes up. This means that at higher energies the detector is able to better discriminate between different energies. The dominant cause of peak broadening is having a low resolution detector. Having gamma-rays that are emitted within the resolution of the

Centroid Channel Number	FWHM	Resolution (keV)	Energy (keV)
122	2.78	0.0228	122.65
1157	2.29	0.00198	1173.2
1314	2.25	0.00171	1332.5
824	2.02	0.00245	834.8
88	1.70	0.0193	88.03
54	0.97	0.0180	53.16
82	1.81	0.0221	81.00
274	1.79	0.00653	276.4
300	1.78	0.00593	302.9
352	1.70	0.00483	356.0
379	1.60	0.00422	383.8

Table 9: Calculated resolutions for prominent gamma spectra peaks.

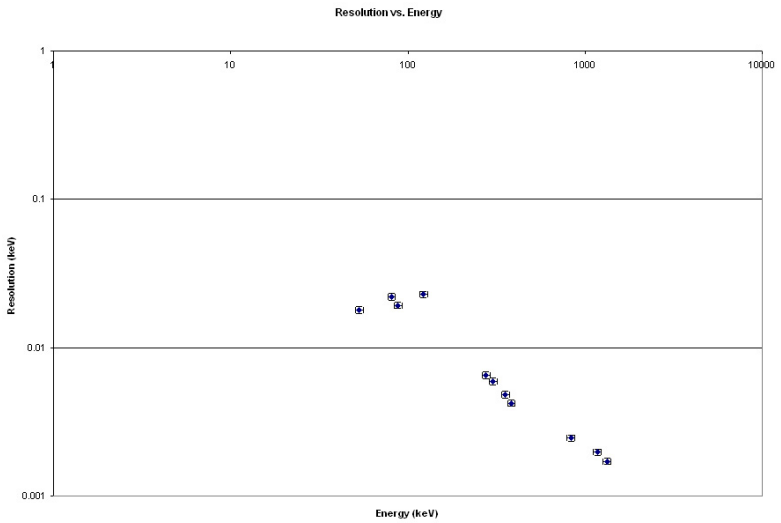

Figure 6.9: A log-log plot of resolution vs. energy.

detector will produce broadened peaks.

Part 8 on the lab instructions asks for the peak-to-total values to be plotted as a function of energy.

Figure 6.10 is the plot of the peak-to-total values as a function of energy. The graph shows

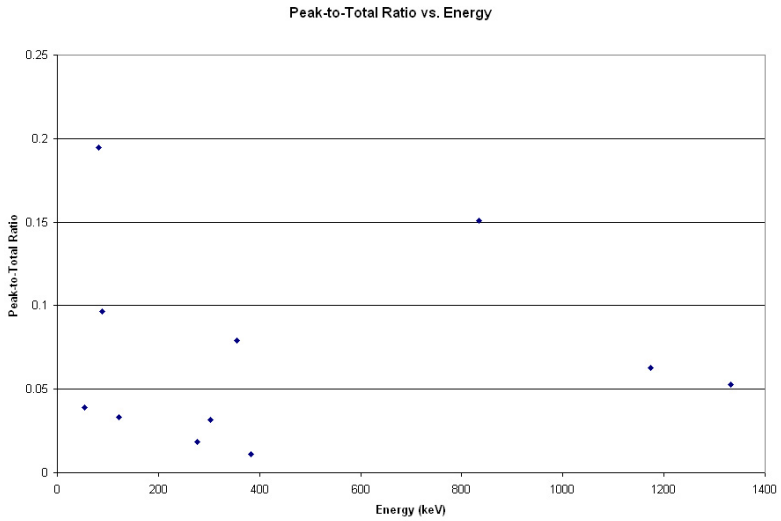

Figure 6.10: Peak-to-total values as a function of energy.

no real correlation between the two different values. There is a cluster of points with small peak-to-total ratios and small energies. This can most likely be explained by the process that most gamma-rays undergo at low energies, photoelectric absorption. Photoelectric absorptions that are detected will produce a low peak-to-total ratio, thus explaining the cluster of points in the lower left of the graph. No other real trends are exemplified by the data.

6.11 Background Analysis

A 15-minute background count was taken in lab[2]. Figure 6.11 is the spectrum that was recorded.

As is done by Knoll, the background spectrum is dissected into three different sections, each consisting of 500 channels. This is done so that the regions of interest can be zoomed in on and its features located more easily.

[2]It should be noted that the background spectrum that was measured became corrupted and that the data analyzed in this section was the measurement of a separate group.

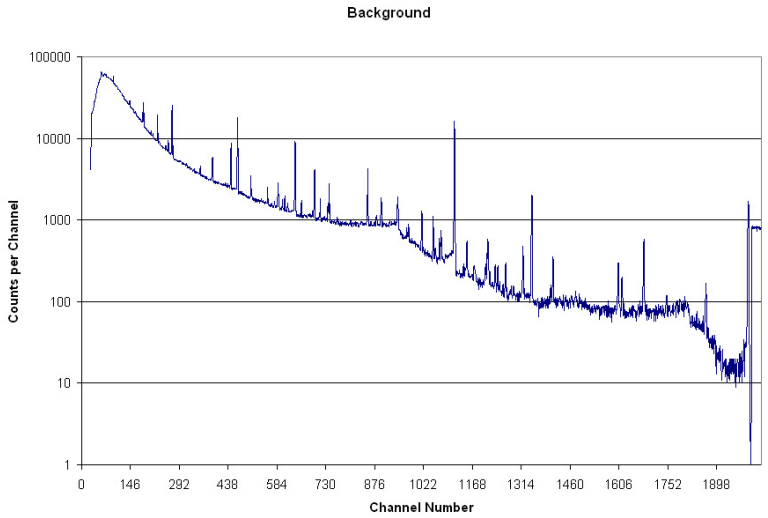

Figure 6.11: The natural background radiation spectrum as it was measured in the laboratory.

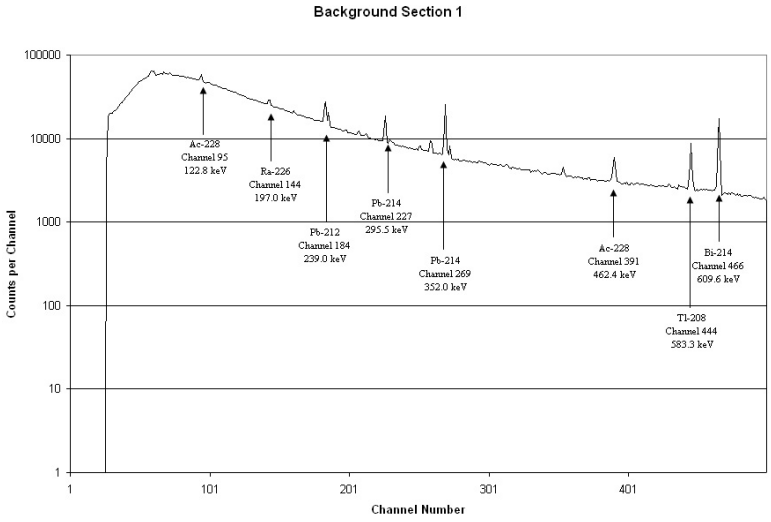

Figure 6.12: Background spectrum over channels 1-500.

Figure 6.12 is the background spectrum that is zoomed in over the first 500 channels. Judging by the total number of nucleons inside all the isotopes that are labeled in Figure 6.12, we can see that they are all daughters of either the ^{232}Th (4n) decay chain or the ^{238}U (4n + 2)

decay chain, commonly known as the radium series. As mentioned in Section 3.8, These isotopes are present in all types of materials, as well as their daughter particles. The most likely source for these isotopes are impurities in the material. The shielding around the detector is made of lead, which has been known to house such impurities. These Thorium and Uranium impurities, as well as ^{40}K, are also present in the detector as impurities as well. It is of note that there are no signs of cosmic radiation on the background spectrum. Cosmic radiation is blocked out by the lead bricks around the detector. The lead bricks have a high atomic number, Z, and this makes them great for blocking cosmic radiation.

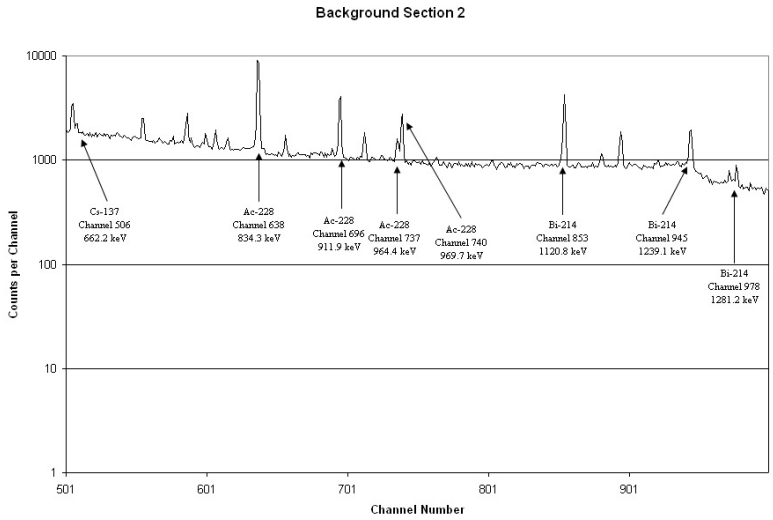

Figure 6.13: Background spectrum over channels 501-1000.

Figure 6.13 is the background spectrum zoomed in over the next 500 channels of the detector. I this figure, all of the same decay chain isotopes are present that were in the previous section of the spectrum, but this time there is the addition of ^{137}Cs. Again, the isotopes that are not Cs come from either the 4n or the 4n + 2 decay chains from impurities in the material. The ^{137}Cs peak is a curious one. ^{137}Cs is a fission product and has been noted as being released into the environment due to weapons testing of the years. It could also

be an impurity that is present inside some of the surrounding material. Also, it as again noted that there is no cosmic radiation present on the spectrum since these cosmic rays are blocked out by the high Z lead bricks.

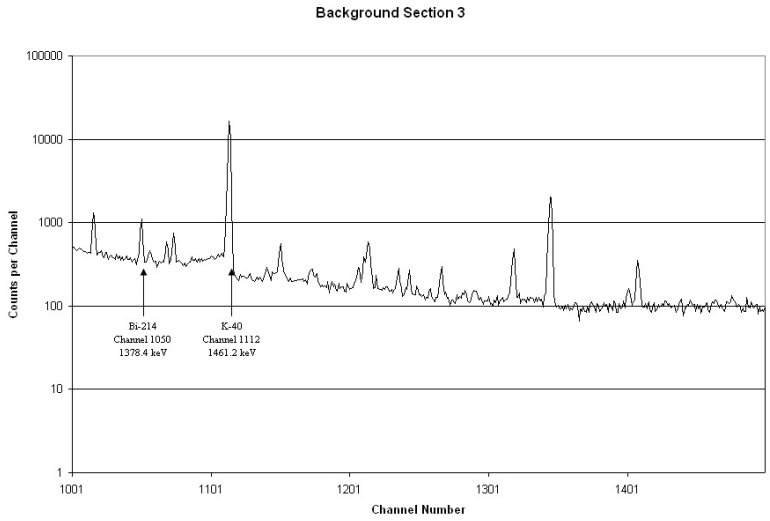

Figure 6.14: Background spectrum over channels 1001-1500.

Figure 6.14 is the background spectrum zoomed in over channels 1001-1500. There were only two identifiable peaks of note in this section of the spectrum. One of them is a member of the radium series decay chain. The other important peak, and the most prominent peak over the entire background spectrum, is the ^{40}K peak. ^{40}K is present in many materials, including bananas, and the materials that make up the detector and the materials that house it are no different in the sense that they too contain ^{40}K due to its extremely large half-life.

There are other peaks that are on this background spectrum, but they are sometimes difficult to identify for certain. The ones that are labeled are the 18 most prominent peaks on the background spectrum and are labeled without any uncertainty.

Table 10 shows the percent error between the measured background peaks and their actual energy values taken from Knoll (pp. 759).

Measured Energy (keV)	Actual Energy (keV)	Percent Error	Source
122.8	129	4.80	^{228}Ac
197	186	5.91	^{226}Ra
239	238.6	0.168	^{212}Pb
295.5	295.2	0.102	^{214}Pb
352	352	0.00	^{214}Pb
462.4	463	0.130	^{228}Ac
583.3	583.2	0.0171	^{208}Tl
609.6	609.3	0.0492	^{214}Bi
662.2	661.6	0.0907	^{137}Cs
834.3	836	0.203	^{228}Ac
911.9	911	0.0988	^{228}Ac
964.4	965	0.0622	^{228}Ac
969.7	969	0.0722	^{228}Ac
1120.8	1120.4	0.0357	^{214}Bi
1239.1	1238.2	0.0727	^{214}Bi
1281.2	1281.1	0.00781	^{214}Bi
1378.4	1377.7	0.0508	^{214}Bi
1461.2	1461	0.0137	^{40}K

Table 10: Measured energies and their agreement with known values for the 18 most prominent background peaks.

This table does not require much comment. By observing the rightmost column, it can be seen that the data collected in the laboratory shows excellent agreement with actual known values of these energies.

7 Conclusions

Through the course of this lab, many gamma spectra were analyzed. In doing so, the features of a gamma spectrum such as photopeaks, summation peaks, annihilation peaks, the

Compton continuum to name a few, are now easily identifiable.

It can also be concluded that there are many radiation sources that are present in the background in everyday life. Most of these sources were from ^{40}K and the daughters of the 4n and 4n + 2 decay chains. In order to analyze an accurate gamma spectrum, this ambient radiation must be accounted for.

The energy resolution of the detector was also observed in the laboratory. The HPGe detector has a very high resolution. For gamma-rays with higher energies this resolution increased.

In all, values from measurements and theory showed much agreement in all facets of this lab.

Appendices

Appendix A ^{57}Co Decay Scheme

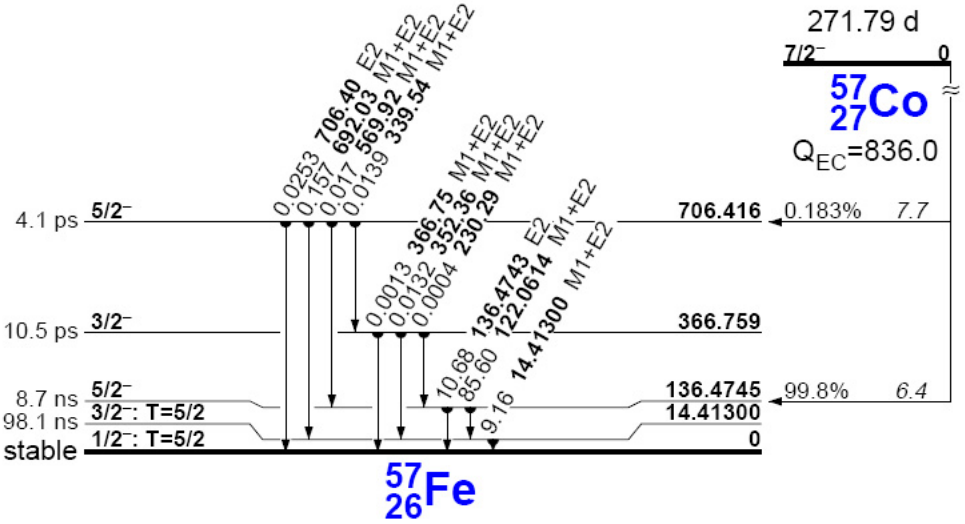

Appendix B ^{60}Co Decay Scheme

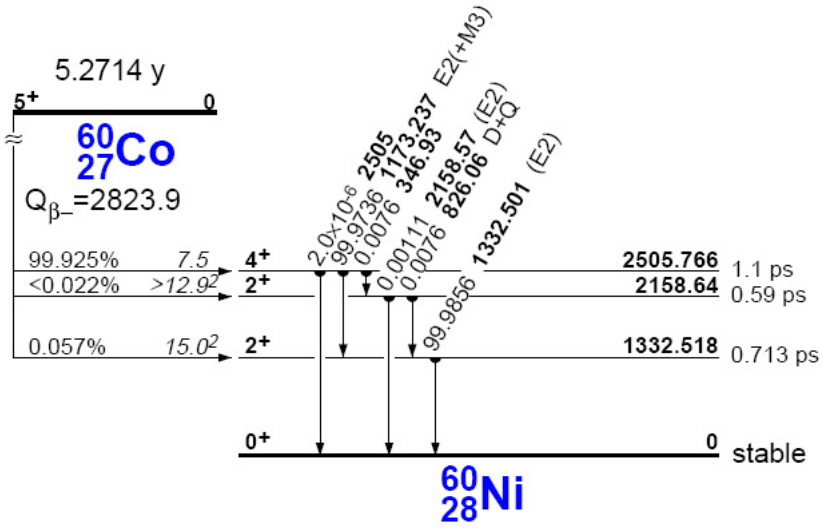

Appendix C ^{137}Cs Decay Scheme

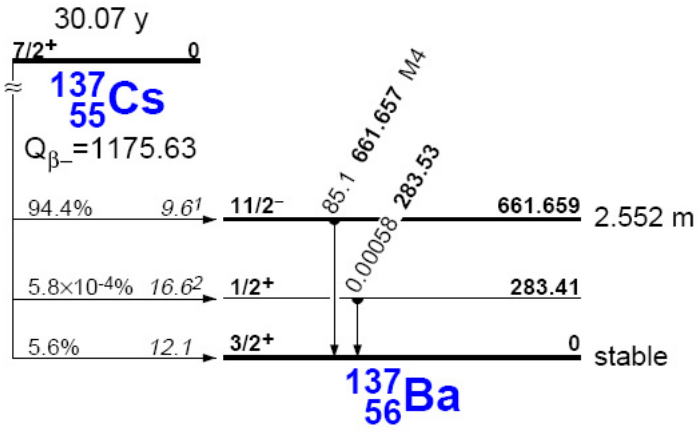

Appendix D ^{22}Na Decay Scheme

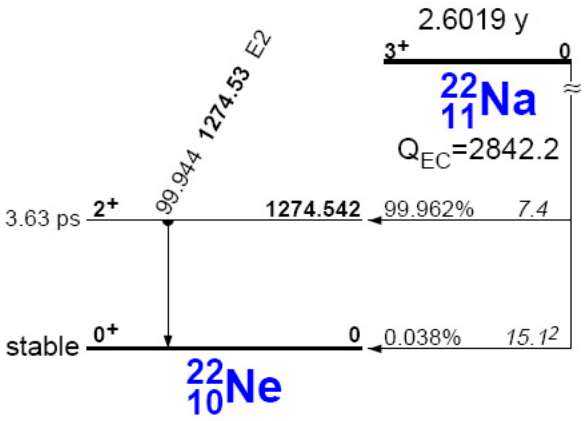

Appendix E ^{133}Ba Decay Scheme

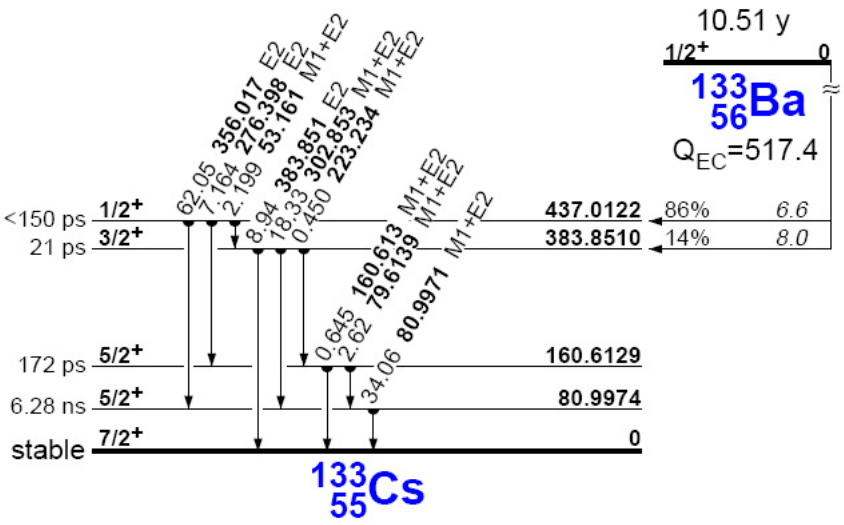

Appendix F ^{109}Cd Decay Scheme

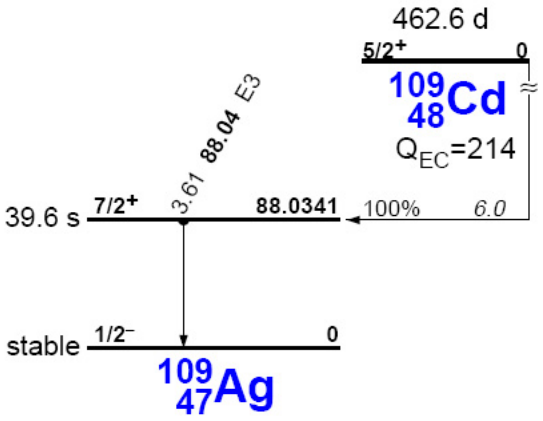

Appendix G ^{54}Mn Decay Scheme

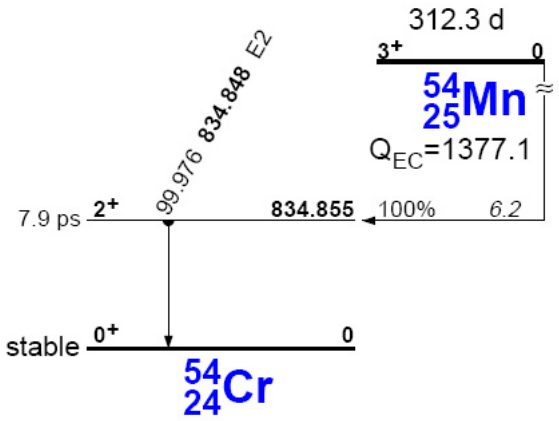

Appendix H HPGe Detector Apparatus

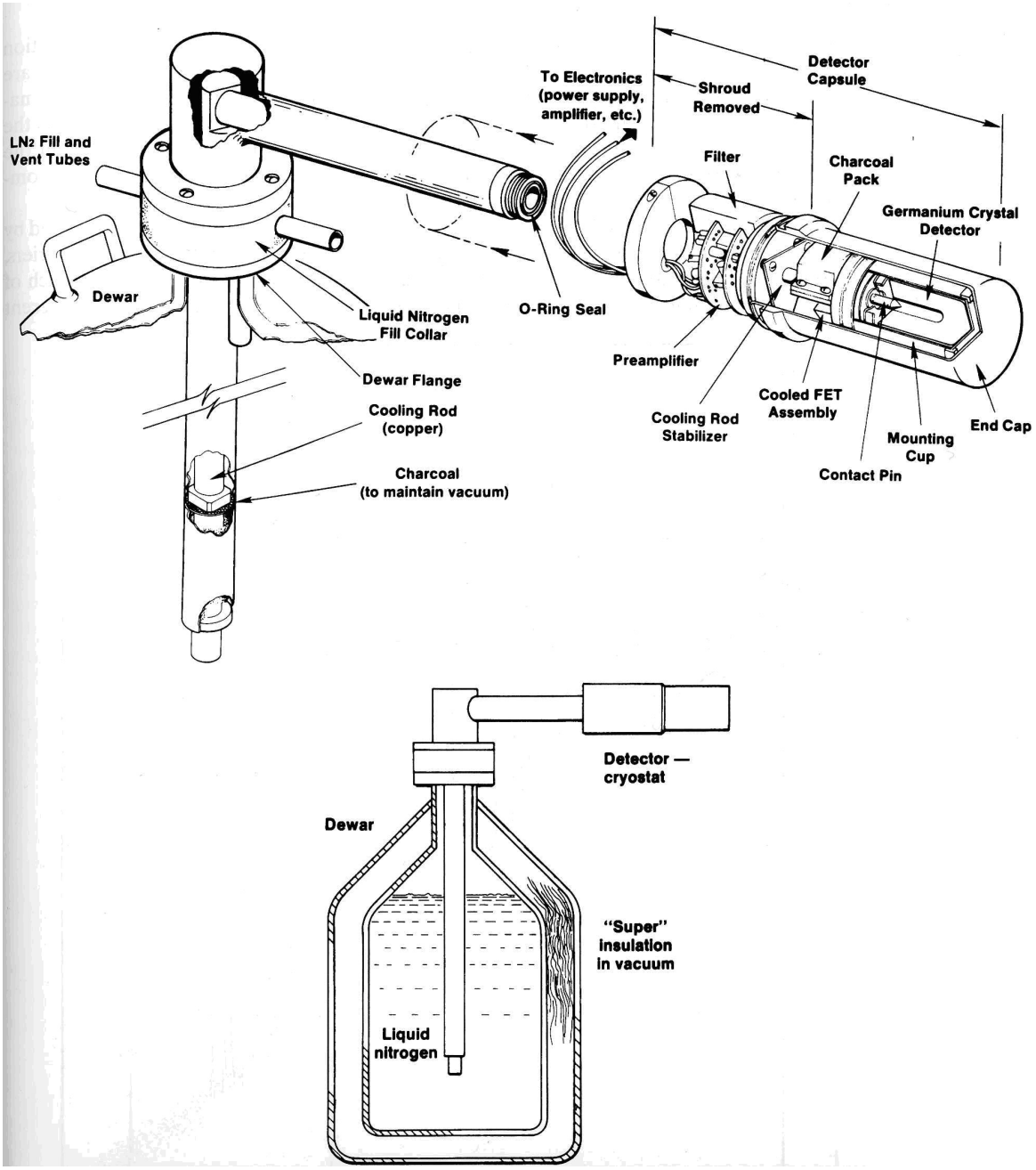

Figure H.1: Diagram showing the location of a HPGe detector with its vacuum capsule.

Appendix I Raw Gamma-Ray Spectra

All of the gamma-ray spectra that were analyzed throughout the course of this lab are available at:

`http://www-personal.umich.edu/ ianrit/downloads/gammaspecspectrums/`

References

[1] Glenn F. Knoll, Radiation Detection and Measurement. John Wiley & Sons, Inc., USA, 3rd Edition, 2000.

[2] Knolls Atomic Power Laboratory, Nuclides and Isotopes: Chart of the Nuclides. Lockheed Martin, USA, 16th Edition, 2002.

[3] Bernard Shleien, Lester A. Slaback, Brian Kent Birky, Ed., Handbook of Health Physics and Radiological Health. Williams & Wilkins, Baltimore MD, 3rd Edition, 1998.